Neutron suppression in polarized *dd* fusion reaction

J. S. Zhang,* K. F. Liu, and G. W. Shuy
Department of Physics and Astronomy, University of Kentucky, Lexington, Kentucky 40506
(Received 9 April 1999; published 18 October 1999)

We report a model-independent partial-wave analysis of polarized dd fusion reactions at low energies. The radial transition amplitudes, designated by the central, spin-orbit, and tensor forces, are determined by fitting angular distributions of the tensor and vector analyzing powers $A_{XZ}(\theta)$, $A_{ZZ}(\theta)$, $A_{XX\text{-}YY}(\theta)$, and $A_Y(\theta)$, and the unpolarized cross section $\sigma_0(\theta)$. The polarized fusion cross section $\sigma_{1,1}(\theta)$ is then predicted from these radial transition amplitudes. We stress that this is feasible only when these amplitudes are separated according to the tensor rank of the interaction. This study includes the *D*-state components of the deuteron, triton, and ^{3}He, and the partial-wave expansion is done up to the d wave for both the entrance and exit channels. Experimental data at $E_{\rm lab}=30$, 50, 70, and 90 keV for the $d(d,p)t$ reaction are very well fitted with this method. It is found that the ratio of polarized to unpolarized cross sections is about 86% at 30 keV and goes down to 22% at 90 keV. The implication of the suppression of a polarized dd fusion reaction is discussed in the context of the neutron-lean fusion reactor with polarized D-^{3}He fuel. It turns out that the important range of energy for suppressing the $d(d,p)t$ and $d(d,n)^3He$ reactions at the plasma temperature $T=60$ keV is $E_d=80$–600 keV. More experimental data are needed in this range to make a detailed study of the neutron suppression. [S0556-2813(99)04409-X]

PACS number(s): 25.10.+s, 24.10.−i, 24.70.+s, 28.52.Cx

I. INTRODUCTION

It has been suggested [1,2] that the spin degree of freedom plays a role which allows certain reaction channels in plasma fusion reactions to be selectively enhanced or suppressed. In particular, if the polarized $\vec{d}(\vec{d},n)^3$He and $\vec{d}(\vec{d},p)t$ cross sections are indeed suppressed by choosing the deuteron spin to be parallel to each other to reduce the secondary neutrons and tritons, the idea of a *neutron-lean* fusion reactor based on polarized D-^{3}He fuel with a predominant ^{3}He$(d,p)^4$He reaction would be appealing [1–4].

An early partial-wave analysis [5] of the experimental data of the $d(d,p)t$ reaction with a polarized deuteron beam in the energy range 100–500 keV suggests that the quintet state $^5S_2$ in the entrance channel is small compared to the singlet state $^1S_0$. This suppression is thought to occur when the deuterons are polarized in parallel (i.e., $S=2$) so that at low energies where the relative s wave dominates, the Pauli principle would impede the reaction. However, it was pointed out by Hofmann and Fick [6] that the inclusion of the *D*-state probability in ^{3}He allows the strong central force to contribute to the $S=2$ channel. As a result, they predicted nonsuppression of the ratio of the polarized to unpolarized cross section $\sigma_{1,1}/\sigma_0$ in their refined resonating-group method (RGM) calculation [6]. A similar conclusion is reached from the *R*-matrix analysis by Hale and Doolen [7,8]. On the other hand, the distorted-wave Born approximation (DWBA) calculation performed by the present authors [9] shows that the ratio $\sigma_{1,1}/\sigma_0$ is only 8% in the range 20–150 keV despite the inclusion of the *D*-state component in ^{3}He. These conflicting conclusions have left theoretical studies in a quandary. Added to the controversy is the following twist. Abu-Kamer *et al.* [10] investigated the dependence of the wave function and interaction in a one-step $d(d,n)^3$He reaction calculation and pointed out that the Gaussian-type potential and deuteron wave function used in both the DWBA [9] and the RGM [6] calculations are not realistic. In particular, when a consistent deuteron wave function and deuteron-^{3}He overlap function are used together with the Reid potential in a one-step reaction model, it is found [10] that the unpolarized cross section is overestimated by two orders of magnitude, whereas the DWBA result [9] is reproduced when the afore-mentioned Gaussian potential and wave functions are used. This has raised doubts in the theoretical studies at these low energies.

In view of the above unsatisfactory and unsettling status of the theoretical calculations, we undertake a partial-wave analysis of the $d(d,p)t$ reaction for the unpolarized, singly polarized, and doubly polarized cross sections. What sets our partial-wave analysis formalism apart from previous analyses [5,11–13] is that the matrix elements are explicitly separated according to the tensor rank of the NN interaction. This is necessary for the prediction of the doubly polarized cross section, since these matrix elements appear in different combinations in the singly and doubly polarized cross sections.

The values and relative phases of the radial matrix elements are determined by fitting the data from the unpolarized cross section $\sigma_0(\theta)$, the three tensor analyzing powers $A_{ZZ}(\theta)$, $A_{XZ}(\theta)$, and $A_{XX\text{-}YY}(\theta)$, and the vector analyzing power $A_Y(\theta)$ from the singly polarized cross section $\sigma_{1,0}$. The doubly polarized cross section $\sigma_{1,1}$ is then predicted from these radial matrix elements. Partial waves are expanded up to d wave which is sufficient for the energy range we consider, $E_{\rm lab}=30$–90 keV. Furthermore, we have included the *D*-state contributions of the deuteron, triton, and ^{3}He. Since this is a partial-wave analysis which includes all multistep processes, it should yield model-independent results as judged by how well the experimental data are fitted.

*On leave from Institute of Atomic Energy, Beijing, China.

We found that $\sigma_{1,1}$ is unsuppressed at very low energy, i.e., $\sigma_{1,1}/\sigma_0 = 0.86$ at $E_{\rm lab} = 30$ keV. Indeed, as suggested by Hofmann and Fick [6], this is mainly due to the *D*-state component in ^{3}He and *t* which is connected to the $^5S_2$ incoming channel through the central force. However, as energy increases, this ratio decreases and goes down as low as 22% at $E_{\rm lab} = 90$ keV. This is much lower than those predicted from the RGM [6] and the *R*-matrix analysis [7,8].

This paper is organized as follows. Section II defines the partial-wave expansion of the wave functions in the $d(d,p)t$ reaction and the transition amplitudes associated with different channels and the type of *NN* interaction. The radial transition amplitudes are then fitted to experimental data of unpolarized and singly polarized cross sections in Sec. III. With these transition amplitudes, we predict, in Sec. IV, the doubly polarized cross section $\sigma_{1,1}$ in the energy range $E_{\rm lab} = 30$–90 keV. Section V discusses the neutron suppression in the thermal fusion reactor environment with polarized *D*-^{3}He fuel. Finally, we summarize our study in Sec. VI.

II. PARTIAL-WAVE EXPANSION OF WAVE FUNCTIONS AND TRANSITION AMPLITUDES

The deuteron fusion reactions $d(d,p)t$ and $d(d,n)^3$He are typical examples of the re-arrangement collision process, where a proton or a neutron is transferred from one deuteron to the other in the nuclear collision process. This process is a subset of the nuclear collision processes that can be labeled as

$$a + A = b + B, \tag{1}$$

where *a* and *A* refer to the incident and target nuclei, while *b* and *B* represent the product nuclei after the collision. The rearrangement collision process can be described as some nucleons being transferred from *a* to *A* (or *A* to *a*). The differential cross section of the rearrangement collision in the center-of-mass system can be described as

$$\frac{d\sigma}{d\Omega_b} = \frac{\mu_a \mu_b k_b}{(2\pi\hbar)^2 k_a} \frac{2}{(2S_a+1)(2S_A+1)} \times \sum_{m,m',\ldots} |\langle \Phi_b | V | \Psi_a^{(+)} \rangle|^2, \tag{2}$$

where μ_a, μ_b and k_a, k_b stand for the reduced masses and wave vectors for the incoming and outgoing channels, and S_a and $\Psi_a^{(+)}$ refer to the channel spin and wave function of the incoming channel. The incoming wave function $\Psi_a^{(+)}$, a function of the relative coordinate $\vec{r}_a$ between *a* and *A* and the intrinsic coordinates in *a* and *A* as labeled by ξ, is the solution of the Lippmann-Schwinger equation

$$\Psi_a^{(+)}(\vec{r}_a, \xi) = \Phi_a + (E_a - H_a + i\eta)^{-1} V \Psi_a^{(+)}(\vec{r}_a, \xi), \tag{3}$$

where E_a and H_a are the energy and Hamiltonian of the incoming channel, and Φ_a is the unperturbed incoming wave function.

Unlike the DWBA which approximates the $\Psi_a^{(+)}$ by a distorted wave function due to the optical potential in the incoming channel and is a one-step process as far as the nucleon transfer reaction is concerned, our present study expands the full transition amplitude $\langle \Phi_b | V | \Psi_a^{(+)} \rangle$ in the partial waves of the incoming and outgoing channels. The *D* components in the internal wave functions of the deuteron, *t*, and ^{3}He are also included. Furthermore, we separate out the matrix elements due to the central, spin-orbit, and tensor interactions. As will be shown in Sec. IV, this separation according to the tensor rank of the *NN* interaction is essential in evaluating the polarized cross section $\sigma_{1,1}$. After these steps are taken, the only unknowns in the differential cross sections are the radial transition amplitudes due to the potential *V*. The complex radial transition amplitudes can be obtained by fitting the angular distributions of the unpolarized and beam polarized differential cross sections. Finally, the polarized cross section is calculated from these radial matrix elements. To the extent that the partial-wave analysis is valid at the low energy we are concerned with, i.e., $E_{\rm lab} = 30$–90 keV, the present approach is free from the theoretical uncertainties we alluded to in the Introduction. It should give a model-independent prediction of $\sigma_{1,1}$, provided that $\sigma_0(\theta)$ and $\sigma_{1,0}(\theta)$ can be reasonably well fitted with the prescribed partial waves.

In the rest of this section, we derive the partial-wave expansion of the transition amplitudes of the $d(d,p)t$ reaction. These amplitudes describe the rearrangement collision of the deuteron beam on the deuteron target, where one deuteron (beam or target nucleus) picks up the neutron of the other deuteron to form a triton. All the formulas given in the following for the $d(d,p)t$ reaction are also valid for the $d(d,n)^3$He reaction provided that one makes appropriate exchanges in the particle labels. In Sec. II A, we define the particle labels and prescribe the antisymmetrization operator for the wave function of the $d+d$ system. The two-body interaction potentials are also discussed. In Sec. II B, we define the relative coordinates and the intrinsic coordinates for the $d(d,p)t$ reaction, and derive the partial-wave expansion for the entrance and exit wave functions in these coordinates. Sec. II C, we define the transition amplitudes, list all the possible nuclear interactions within the framework of this study, and then derive a common form for the transition amplitudes that separately describes the contributions of different nuclear interaction forces, total angular momenta, and intrinsic states of the final product (triton or ^{3}He).

A. Particle labeling, antisymmetrization, and two-body interaction potential

Unless otherwise indicated, this paper assigns particles 1 and 3 as protons and particles 2 and 4 as neutrons in the $d(d,p)t$ reaction channel. The total spins of the incoming and outgoing channels are denoted as $S_{\rm in}$ and $S_{\rm out}$. The magnetic quantum numbers of the two deuterons are *m* and *n* in the incident state, while m' and n' denote the coupled spin magnetic quantum numbers of the (1,2) and (3,4) pairs in the exit channel, i.e., *p* and *t*.

Since we distinguish the protons from the neutrons, the antisymmetrization only involves the permutation between the protons and neutrons separately. This is done with the antisymmetrization operator on the wave function of the $d+d$ system which can be written as

$$\mathcal{A}=\frac{1}{2}(1-P_{13})(1-P_{24})=\frac{1}{2}(1-P_{13})(1+P_{13}P_{24}),$$

$$=\frac{1}{2}[1+(-)^{L_{\rm in}+S_{\rm in}}](1-P_{13}). \quad (4)$$

The last step reflects the Bose symmetry between the two deuterons in the incoming channel. The two-body nucleon interaction potential V contains the central force, the spin-orbit force, and the tensor force. The central force conserves both the spins ($\Delta S=0$) and the orbital angular momentum ($\Delta L=0$). The spin-orbit force can lead to spin ($\Delta S=1$) and orbital angular momentum flip ($\Delta L=1$). The tensor force can flip the spin and orbital angular momentum up to two units, i.e., $\Delta S=2$ and $\Delta L=2$. The two-body transition potential V in Eq. (2) for the $d+d$ rearrangement collision to the final product of a proton (particle 3) and a triton (particles 1, 2, and 4) is described by

$$V=V(1,3)+V(2,3)+V(3,4)-U[\vec{r}_3-(\vec{r}_1+\vec{r}_2+\vec{r}_4)/3], \quad (5)$$

where $V(i,j)$ is the interaction potential between i and j, and $U[\vec{r}_3-(\vec{r}_1+\vec{r}_2+\vec{r}_4)/3]$ is the average potential acting on the particle 3 (proton) from particles 1, 2, and 4 in the triton. In the present analysis, we have included the contribution of the dominant interaction $V(3,4)$ in the partial-wave analysis but neglected the contribution of $V(1,3)+V(2,3)-U[\vec{r}_3-(\vec{r}_1+\vec{2}_2+\vec{r}_4)/3]$. This is usually done in DWBA calculations of stripping and pickup reactions involving heavy targets. The same approximation is made here as in the one-step reaction calculation [10]. We have checked that the neglected interaction does not give rise to a dominant polynomials in the Legendre expansion of the experimental analyzing powers. Thus we believe it should be small compared with the contribution from $V(3,4)$.

B. Partial-wave expansion of wave functions

The relative coordinates of the four-nucleon system are chosen as follows:

$$\vec{R}_c=\frac{1}{4}(\vec{r}_1+\vec{r}_2+\vec{r}_3+\vec{r}_4),$$

$$\vec{R}_\alpha=\frac{1}{2}(\vec{r}_1+\vec{r}_2)-\frac{1}{2}(\vec{r}_3+\vec{r}_4),$$

$$\vec{r}=\vec{r}_1-\vec{r}_2,$$

$$\vec{r}'=\vec{r}_3-\vec{r}_4, \quad (6)$$

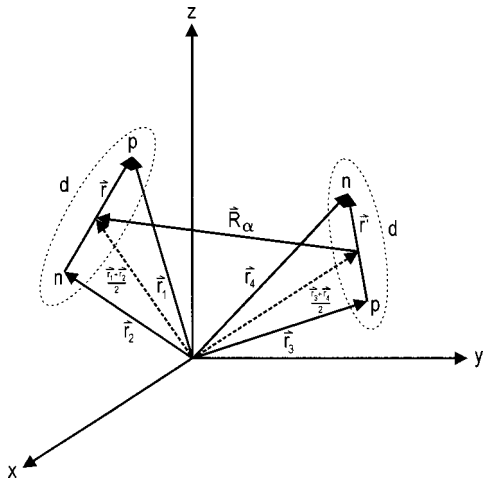

FIG. 1. The relative coordinate $\vec{R}_\alpha$ between the two deutrons and the deuteron intrinsic coordinates $\vec{r}$ and $\vec{r}'$ as defined in Eq. (6) are plotted in the center-of-mass system with $\vec{R}_c=$const.

where $\vec{R}_c$ is the center-of-mass coordinate, $\vec{R}_\alpha$ is the relative coordinate between the two deuterons, and $\vec{r}$ and $\vec{r}'$ are the intrinsic coordinates of the two deuterons. We show these coordinates in Fig. 1 in the center of mass system where $\vec{R}_c$ is constant. Any other relative coordinates can be described in terms of $\vec{R}_\alpha$, $\vec{r}$, and $\vec{r}'$. For example, the relative coordinate between p and triton (similarly for n and ^{3}He) is

$$\vec{R}_\beta=\frac{1}{3}(\vec{r}_1+\vec{r}_2+\vec{r}_4)-\vec{r}_3=\frac{2}{3}(\vec{R}_\alpha-\vec{r}') \quad (7)$$

and the relative coordinate between n and d in the triton (similarly for p and d in ^{3}He) is

$$\vec{R}_h=\frac{1}{2}(\vec{r}_1+\vec{r}_2)-\vec{r}_4=\vec{R}_\alpha+\frac{1}{2}\vec{r}'. \quad (8)$$

In the following, the wave functions for the entrance and exit channels of the $d(d,p)t$ reaction are expressed in terms of these coordinates.

The relative wave function between the deuterons in the entrance channel with angular momentum L is

$$\chi^{(+)}_{L0}(\vec{k}_{\rm in}\cdot\vec{R}_\alpha)=\chi^{(+)}(R_\alpha)Y_{L,0}(\Omega_\alpha), \quad (9)$$

where we have taken the incoming relative momentum $\vec{k}_{\rm in}$ to be along the Z axis and Ω_α represent the angles between $\vec{k}_{\rm in}$ and R_α. $\chi^{(+)}(R_\alpha)$ is the radial wave function. The exchange wave function can be written in terms of the coordinates $\vec{r}$ and $\vec{r}'$

$$\chi^{(+)}_{L0}(\vec{k}_{\rm in}\cdot P_{13}\vec{R}_\alpha)=\chi^{(+)}_{L0}[\vec{k}_{\rm in}\cdot(\vec{r}'-\vec{r})/2]=\sum_{l_1,l_2}\chi^{(+)}_{l_1,l_2}(r,r')$$
$$\times\Bigg[\sum_{m_1}\sqrt{4\pi(2l_1+1)}Y^*_{l_1m_1}(\Omega_{\rm in})$$
$$\times Y_{l_1m_1}(\Omega_r)\sum_{m_2}\sqrt{4\pi(2l_2+1)}$$
$$\times Y^*_{l_2m_2}(\Omega_{in})Y_{l_2m_2}(\Omega_{r'})\Bigg]_{L0}$$
$$=\sum_{l_1,l_2}\chi^{(+)}_{l_1l_2}(r,r')\sum_{m_l}C(l_1,l_2,L;$$
$$-m_l,m_l,0)C(l_1,l_2,L;0,0,0)Y_{l_1,-m_l}(\Omega_r)$$
$$\times Y_{l_2,m_l}(\Omega_{r'}),\qquad(10)$$

where $\chi^{(+)}_{l_1l_2}(r,r')$ is the exchange radial wave function and $C(l_1,l_2,L;m_1,m_2,M=m_1+m_2)$ is the Clebsch-Gordon coefficient which reflects the fact that l_1,m_1 and l_2,m_2 are coupled to $L0$. Ω_r and $\Omega_{r'}$ are the solid angles of the coordinates $\vec{r}$ and $\vec{r}'$, respectively. In going to the last step, we have used the fact that the incoming relative momentum $\vec{k}_{\rm in}$ is along the Z axis, and hence $\Omega_{\rm in}$ corresponds to $\theta=0$.

The p-t relative wave function with relative coordinate R_β in the exit channel with angular momentum L' and M' is written as follows:

$$\chi^{(-)}_{L',M'}(\vec{k}_{\rm out}\cdot\vec{R}_\beta)$$
$$=\chi^{(-)}_{L',M'}(\vec{k}_{\rm out}\cdot\vec{R}_\alpha,\vec{k}_{\rm out}\cdot\vec{r}')=\sum_{l,l'}\mathcal{L}^{(-)}_{ll'}(k_{\rm out},R_\alpha,r')$$
$$\times\Bigg[\sum_m\sqrt{4\pi(2l+1)}Y^*_{lm}(\Omega)Y_{lm}(\Omega_\alpha)$$
$$\times\sum_{m'}\sqrt{4\pi(2l'+1)}Y^*_{l'm'}(\Omega)Y_{l'm'}(\Omega_{r'})\Bigg]_{L'M'}$$
$$=\sum_{ll'}\sqrt{\frac{4\pi}{2L'+1}}\mathcal{L}^{(-)}_{ll'}(k_{\rm out},R_\alpha,r')$$
$$\times\sum_m C(l,l',L';m,M'-m,M')$$
$$\times C(l,l',L';0,0,0)Y_{l,m}(\Omega_\alpha)$$
$$\times Y_{l',M'-m}(\Omega_{r'})Y^*_{L',M'}(\Omega),\qquad(11)$$

where Ω refers to the angle between $\vec{k}_{\rm in}$ and $\vec{k}_{\rm out}$ and $\mathcal{L}^{(-)}_{ll'}(k_{\rm out},R_\alpha,r')$ is the radial wave function of the exit channel. l and l' are the orbital angular momenta associated with the solid angles Ω_α and $\Omega_{r'}$.

The wave functions of the intrinsic states of t (similarly for ^{3}He) with S- and D-state components are

$$\varphi^S_t(\vec{r},\vec{R}_h)=\sum_{l_h,m_h}\varphi^S_{l_h}(R_\alpha,r,r')C(l_h,l_h,0;m_h,-m_h,0)$$
$$\times Y_{l_h,m_h}(\Omega_\alpha)Y_{l_h,-m_h}(\Omega_{r'}),$$

$$\varphi^D_t(\vec{r},\vec{R}_h)_{m_D}=\sum_{l_h,m_h}\varphi^D_{l_h}(R_\alpha,r,r')$$
$$\times C(l_h,l_h,2;m_h,m_D-m_h,m_D)$$
$$\times Y_{l_h,m_h}(\Omega_\alpha)Y_{l_h,m_D-m_h}(\Omega_{r'}),\qquad(12)$$

where $\vec{R}_h$ is the coordinate between n and d in the triton as shown in Eq. (8). $\varphi^S_{l_h}(R_\alpha,r,r')$ and $\varphi^D_{l_h}(R_\alpha,r,r')$ are the radial wave functions of the S- and D-state components, respectively, and the subscript m_D is the magnetic quantum number of the D-state component in the t or ^{3}He. Here we consider the D wave between n and deutron as the only source of D-state component of t. The D-state component of t with the intrinsic deutron in the D state is neglected. The transition involving intrinsic deutrons in the D state for both the entrance and exit channels is very small. Furthermore, there is no transition to the triton with its subdeutron in the D state from the S-state deutron in the entrance channel, because interaction $V(3,4)$ does not involve particles 1 and 2 in the deutron and the wave functions are orthogonal in this case.

The exchange term of the product of the S-state (intrinsic state) wave functions of the two deuterons in the incoming channel is

$$\varphi^S_d(2P_{13}\vec{r})\varphi^S_d(2P_{13}\vec{r}')$$
$$=\varphi^S_d(\vec{r}+\vec{r}'-2\vec{R}_\alpha)\varphi^S_d(\vec{r}+\vec{r}'+2\vec{R}_\alpha)$$
$$=\sum_{L_\alpha=\rm even}\sum_{L_r+L'_r=\rm even}\varphi^{SS}_{d+d}(R_\alpha,r,r')_{L_\alpha,L_r,L_{r'}}$$
$$\times\sum_{M_\alpha M_r}(-1)^{M_\alpha}C(L_\alpha,L_r,L_{r'};M_\alpha,-M_r,M_\alpha-M_r)$$
$$\times Y^*_{L_r,M_r}(\Omega_r)Y_{L_\alpha,M_\alpha}(\Omega_\alpha)Y_{L_{r'},M_r-M_\alpha}(\Omega_{r'}),\qquad(13)$$

where $\varphi^{SS}_{d+d}(R_\alpha,r,r')_{L_\alpha,L_r,L_{r'}}$ is the product of radial wave functions with the Legendre expansion rank $L_\alpha,L_r,L_{r'}$ for the angles Ω_α, Ω_r, and $\Omega_{r'}$.

TABLE I. Radial transition amplitudes and the associated channel orbital angular momenta, spin, total channel angular momentum J, and the type of NN interactions are listed. The second and third columns indicate the intrinsic state of the deutron and the triton, respectively.

$\mathcal{R}^{S(D)S(D)}_{L,L',S_{\rm in}}(I)$	d state	t state	$L_{\rm in}$	$L_{\rm out}$	$S_{\rm in}$	$S_{\rm out}$	J^π	Force type
$\mathcal{R}^{SS}_{0,0,0}(0)$	S	S	0	0	0	0	0^+	C
$\mathcal{R}^{SS}_{2,0,2}(2)$			2	0	2	0,1	$0^+,1^+$	T
$\mathcal{R}^{SS}_{1,1,1}(0,1,2)$			1	1	1	1	0^-	C,LS,T
$\mathcal{R}^{SS}_{1,1,1}(0,1,2)$			1	1	1	0,1	1^-	C,LS,T
$\mathcal{R}^{SS}_{1,1,1}(0,1,2)$			1	1	1	1	2^-	C,LS,T
$\mathcal{R}^{SS}_{2,2,2}(1,2)$			2	2	2	0,1	2^+	LS,T
$\mathcal{R}^{SS}_{0,2,2}(2)$			0	2	2	0,1	2^+	T
$\mathcal{R}^{SS}_{2,2,0}(0,1,2)$			2	2	0	0,1	2^+	C,LS,T
$\mathcal{R}^{SD}_{0,2,2}(0)$	S	D	0	2	2	2	2^+	C
$\mathcal{R}^{SD}_{0,2,2}(1)$			0	2	2	1,2	2^+	LS
$\mathcal{R}^{SD}_{0,2,2}(2)$			0	2	2	1,2	2^+	T
$\mathcal{R}^{DS}_{0,2,0}(0,1,2)$	D	S	0	2	0	0,1	2^+	C,LS,T
$\mathcal{R}^{DS}_{0,0,2}(2)$			0	0	2	0,1	$0^+,1^+$	T
$\mathcal{R}^{DS}_{0,2,2}(1,2)$			0	2	2	0,1	2^+	LS,T

The direct product of the intrinsic wave functions of the two deuterons with one in the S state and the other in the D state is

$$\varphi^{d+d}_{n,m}=C(1,1,S_\alpha;n,m,n+m)\times\sum_{m_d}C(1,2,1;m,m_d,m+m_d)\times[\varphi^S_d(r)\varphi^D_d(r')Y_{2,m_d}(\Omega_{r'})+\varphi^S_d(r')\varphi^D_d(r)Y_{2,m_d}(\Omega_r)], \tag{14}$$

where φ^S_d and φ^D_d stand for the direct intrinsic radial wave functions. We shall neglect the exchange matrix elements due to the D-state component in the deuteron in this study. This is justifiable since the D-state component of the deuteron has little effect in the fusion reaction as we will show later through the fit of the experimental data.

Finally, the total wave function is the product of the channel wave function and the intrinsic wave function:

$$\Psi(\Phi)=\chi\varphi. \tag{15}$$

C. Partial-wave expansion of transition amplitudes

The transition amplitude of the reaction $d(d,p)t$ is defined by

$$M_{mm',nn'}(\vec{k}_{\rm in},\vec{k}_{\rm out})=\sqrt{\frac{2\mu_a\mu_b k_b}{(2\pi\hbar)^2k_a}}\langle\Phi_{p+t}(n',m')|V(34)|\mathcal{A}\Psi^{(+)}_{d+d}(n,m)\rangle, \tag{16}$$

where m and n refer to the spins of the two deuterons consisting of nucleons (1,2) and (3,4) in the entrance channel, while m' and n' refer to the spins of the same nucleons (1,2) and (3,4) in the exit channel of p and t.

After the integration over isospin, spin, and angles Ω_α, Ω_r, and $\Omega_{r'}$ are carried out, the transition amplitude M depends only on the radial integrals and the scattering angle Ω. The allowed radial transition amplitudes can be classified according to the s, p, and d partial waves, the S and D components of the intrinsic deuteron and triton, and the tensor rank of the NN interaction. These are listed in Table I together with 20 complex radial transition amplitudes which are denoted as $\mathcal{R}^{S(D)S(D)}_{L,L',S_{\rm in}}(I)$ with $I=0,1,2$ for the central, spin-orbit, and tensor force, respectively. The first superscript of $\mathcal{R}$ denotes the intrinsic states in the deuterons (S stands for S states in both deuterons and D stands for one in the S state and the other one in the D state), while the second one stands for that of the triton (or ^{3}He). The subscripts L and L' denote the orbital angular momenta of the entrance and exit channels, and $S_{\rm in}$ denotes the spin in the incoming channel. Note that the radial transition amplitudes do not depend on $S_{\rm out}$. We further note that for the D-state components of d and t only the s incoming wave is considered. Furthermore, the transition from the deuteron D state to the triton D state is neglected as this involves the product of D-state probabilities in the deutron and triton which is very small.

Using the notation of the radial integrals defined above, the transition amplitude M can be written in the following form. For the case of an S-state component in the intrinsic wave functions of both the deuteron and triton, the transition amplitude is written as

$$M^{(SS)J}_{mm',nn'}(L_{\rm in},L_{\rm out},S_{\rm in},I)=\sum_{S_{\rm out}} B^S(S_{\rm out})\frac{1}{2}[1+(-1)^{L_{\rm in}+S_{\rm in}}]\delta_{n',n}\mathcal{R}^{SS}_{L_{\rm in},L_{\rm out},S_{\rm in}}(I)$$
$$\times C(S_{\rm out},L_{\rm out},J;n+m',m-m',n+m)C(S_{\rm in},L_{\rm in},J;n+m,0,n+m)$$
$$\times C(1,I,1;m,m'-m,m')C(L_{\rm out},L_{\rm in},I;m-m',0,m-m')$$
$$\times C(1,1,S_{\rm out};n,m',n+m')C(1,1,S_{in};n,m,n+m)Y_{L_{\rm out},m-m'}(\Omega). \quad (17)$$

For the case of an S state component in the deuteron and D-state component in the triton, M is written as

$$M^{(SD)J=2}_{mm',nn'}(L_{\rm in}=0,L_{\rm out},S_{\rm in}=2,I)=\delta_{n',n}\frac{1}{2}[1+(-1)^{L_{\rm in}+S_{\rm in}}]\sum_{S_{\rm out}}\mathcal{R}^{SD}_{0,L_{\rm out},2}(I)$$
$$\times B^D(S_{\rm out})\sum_{S_h,m_D}(-1)^{m_D}W\left(2,\frac{3}{2},S_h,\frac{1}{2};\frac{1}{2},S_{\rm out}\right)C(2,S_{\rm out},S_h;m_D,n+m',n+m'+m_D)$$
$$\times C(S_{\rm out},L_{\rm out},J;n+m',m-m',n+m)C(S_{\rm in},L_{\rm in},J;n+m,0,n+m)$$
$$\times C(1,1,S_{\rm out};n,m',n+m')C(1,1,2;n,m,n+m)C(1,I,1;m,m'-m,m')$$
$$\times C(I,2,L_{\rm out};m-m',-m_D,m-m'-m_D)$$
$$\times C(S_h,L_{\rm out},2;n+m'+m_D,m-m'-m_D,n+m)Y_{L_{\rm out},m-m'-m_D}(\Omega). \quad (18)$$

For the case of the D-state component in the deuteron and S-state component in the triton, M is written as

$$M^{(DS)J}_{mm',nn'}(L_{\rm in}=0,L_{\rm out},S_{in},I)=\delta_{n',n}\frac{1}{2}[1+(-1)^{S_{\rm in}}]\sum_{S_{\rm out}}\mathcal{R}^{DS}_{0,L_{\rm out},S_{in}}(I)$$
$$\times B^S(S_{\rm out})\sum_{m_d}C(1,1,S_{\rm out};n',m',n'+m')C(1,1,S_{in};n,m,n+m)$$
$$\times C(S_{\rm out},L_{\rm out},J;n'+m',m-m',n+m+m_d)C(S_{\rm in},2,J;n+m,m_d,n+m-m_d)$$
$$\times C(1,I,1;m,m'-m,m')C(I,2,L_{\rm out};m-m',m_d,m-m'+m_d)$$
$$\times C(1,2,1;m,m_d,m+m_d)C(2,2,L_{\rm out};0,0,0)Y_{L_{\rm out},m-m'+m_d}(\Omega). \quad (19)$$

The values of $B^S(S_{\rm out})$ and $B^D(S_{\rm out})$ in the above partial amplitudes are given in Table II.

The total transition amplitude M is simply the sum of the above partial amplitudes:

$$M^J_{mm',nn'}(L_{in},L_{\rm out},S_{\rm in},I)$$
$$=M^{(SS)J}_{mm',nn'}(L_{\rm in},L_{\rm out},S_{\rm in},I)+M^{(SD)J}_{mm',nn'}(L_{\rm in},L_{\rm out},S_{\rm in},I)$$
$$+M^{(DS)J}_{mm',nn'}(L_{\rm in},L_{\rm out},S_{\rm in},I). \quad (20)$$

TABLE II. Values of $B^S(S_{\rm out})$ and $B^D(S_{\rm out})$

$S_{\rm out}$	0	1	2
$B^S(S_{\rm out})$	$\frac{1}{\sqrt{2}}$	$\frac{1}{\sqrt{3}}$	0
$B^D(S_{\rm out})$	0	$\frac{1}{2}$	$\frac{\sqrt{5}}{2}$

III. FITTING OF RADIAL TRANSITION AMPLITUDES TO NUCLEAR DATA

This section describes the procedure leading to the fitting of radial transition amplitudes to the experimental data on $d(d,p)t$ reactions. First, we define the t-matrix description of the unpolarized and beam-polarized cross sections. Next, the unpolarized cross section and the vector and tensor analyzing powers are expressed in terms of the Legendre or associated Legendre polynomials. It is shown that the radial transition amplitudes are related to the coefficients of these polynomials. Finally, a nonliner χ^2 fit is utilized to fit the radial transition amplitudes to the experimental data.

A. T-matrix description of the cross section

The transition matrix representation of an unpolarized cross section is given [14] as

$$\sigma_0(\theta)\equiv\frac{d\sigma_0}{d\Omega}=\frac{1}{9}{\rm Tr}(MM^+). \quad (21)$$

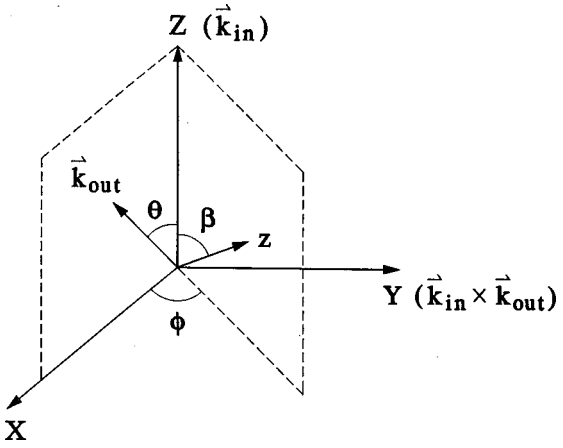

FIG. 2. The beam direction $\vec{k}_{\rm in}$ is set to be along the Z axis. The spin quantization axis is indicated as z. The scattering angle θ and the angles ϕ and β are defined as shown.

The reaction cross section of a polarized beam on an unpolarized target can be expressed [14] as

$$\sigma_{1,0}(\theta,\phi)=\sigma_0(\theta)\Big[1+\frac{3}{2}p_Y A_Y+\frac{2}{3}p_{XZ}A_{XZ}+\frac{1}{2}p_{ZZ}A_{ZZ}+\frac{1}{6}p_{XX\text{-}YY}A_{XX\text{-}YY}\Big], \tag{22}$$

where p_Y, p_{XZ}, p_{ZZ}, and $p_{XX\text{-}YY}$ are the vector and tensor polarizations of the beam, and A_Y, A_{XZ}, A_{ZZ}, and $A_{XX\text{-}YY}$ are the vector and tensor analyzing powers of the transition. They are defined in the following.

A polarized beam can be characterized by the vector and tensor polarizations. To define these polarizations, this study adopts the outgoing reactant helicity frame specified by Ohlson [14]. As shown in Fig. 2, the direction of the incident deuteron $\vec{k}_{\rm in}$ is taken to be along the Z axis, and the $\vec{k}_{\rm out}$ lies in the (X,Z) plane with the scattering angle θ shown in Fig. 2. The Y axis is then normal to the scattering plane, i.e., in the direction of $\vec{k}_{\rm in}\times\vec{k}_{\rm out}$. The quantization axis of the polarized beam is taken to be along its spin direction z which makes an angle β with respect to Z, the direction of $\vec{k}_{\rm in}$. The angle ϕ is defined to be the angle between the plane containing $\vec{k}_{\rm in}$ and $\vec{k}_{\rm out}$ [the plane (X,Z)] and the plane (z,Z).

In this frame, the beam polarization is characterized by

$$p_X=-p_z\sin\beta\sin\phi,$$

$$p_Y=p_z\sin\beta\cos\phi,$$

$$p_Z=p_z\cos\beta,$$

$$p_{XX}=\frac{1}{2}p_{zz}(3\sin^2\beta\sin^2\phi-1),$$

$$p_{YY}=\frac{1}{2}p_{zz}(3\sin^2\beta\cos^2\phi-1),$$

$$p_{ZZ}=\frac{1}{2}p_{zz}(3\cos^2\beta-1),$$

$$p_{XY}=-\frac{3}{2}p_{zz}\sin^2\beta\cos\phi\sin\phi,$$

$$p_{XZ}=-\frac{3}{2}p_{zz}\sin\beta\cos\beta\sin\phi,$$

$$p_{YZ}=\frac{3}{2}p_{zz}\sin\beta\cos\beta\cos\phi,$$

$$p_{XX\text{-}YY}=-\frac{3}{2}p_{zz}\sin^2\beta\cos2\phi, \tag{23}$$

where p_z and p_{zz} are the magnitudes of the vector and tensor polarization.

The analyzing powers are defined in terms of the t matrix M,

$$A_Y(\theta)=\frac{2}{\sqrt{3}}iT_{11}(\theta)=\frac{\mathrm{Tr}(MS_YM^\dagger)}{\mathrm{Tr}(MM^\dagger)},$$

$$A_{ZZ}(\theta)=\sqrt{2}T_{20}(\theta)=\frac{\mathrm{Tr}(MS_{ZZ}M^\dagger)}{\mathrm{Tr}(MM^\dagger)},$$

$$A_{XZ}(\theta)=-\sqrt{3}T_{21}(\theta)=\frac{\mathrm{Tr}(MS_{XZ}M^\dagger)}{\mathrm{Tr}(MM^\dagger)},$$

$$A_{XX\text{-}YY}(\theta)=2\sqrt{3}T_{22}(\theta)=\frac{\mathrm{Tr}(MS_{XX\text{-}YY}M^\dagger)}{\mathrm{Tr}(MM^\dagger)}, \tag{24}$$

where T_{ij} stands for the analyzing powers in the spherical coordinate system. S_X, S_Y, and S_Z are ordinary Cartesian spin 1 operators given explicitly as

$$S_X=\frac{1}{\sqrt{2}}\begin{pmatrix}0&1&0\\1&0&1\\0&1&0\end{pmatrix},\quad S_Y=\frac{i}{\sqrt{2}}\begin{pmatrix}0&-1&0\\1&0&-1\\0&1&0\end{pmatrix},$$

$$S_Z=\begin{pmatrix}1&0&0\\0&0&0\\0&0&-1\end{pmatrix}, \tag{25}$$

whereas operators $S_{ZZ}, S_{XZ}, S_{XX\text{-}YY}=S_{XX}-S_{YY}$ are traceless operators defined as

$$S_{ij}=\frac{3}{2}(S_iS_j+S_jS_i)-2\hat{I}\delta_{ij},\quad i,j=X,Y,Z. \tag{26}$$

B. Polynomial expansion of angular distribution of the unpolarized cross section and analyzing powers

The angular distribution of the unpolarized cross section and the analyzing powers of $d+d$ reactions can be described

by an expansion in Legendre or associated Legendre polynomials. At low energies ($E_{\rm lab} \leqslant 100$ keV), it has been shown experimentally [11–13] that a truncation at $L=4$ gives a very good approximation. The polynomial expansion of the angular distribution of the unpolarized cross section up to $L=4$ is

$$\sigma_0(\theta)=\frac{1}{9}\mathrm{Tr}(MM^{\dagger})\simeq\frac{\sigma_0}{4\pi}\sum_{L=0}^{4} a_L^{\sigma_0}P_L(\cos\theta), \qquad (27)$$

where σ_0 is the total unpolarized $d+d$ reaction cross section. The expansion coefficients $a_1^{\sigma_0}$ and $a_3^{\sigma_0}$ vanish due to the two identical bosons in the entrance channel.

The expansions of the analyzing powers are given in terms of the Legendre and associated Legendre polynomials

$$A_Y(\theta)=\frac{\sigma_0}{4\pi\sigma(\theta)}\sum_{L=1}^{4} a_L^{Y}P_L^1(\cos\theta),$$

$$A_{XZ}(\theta)=\frac{\sigma_0}{4\pi\sigma(\theta)}\sum_{L=1}^{4} a_L^{XZ}P_L^1(\cos\theta),$$

$$A_{ZZ}(\theta)=\frac{\sigma_0}{4\pi\sigma(\theta)}\sum_{L=0}^{4} a_L^{ZZ}P_L(\cos\theta),$$

$$A_{XX\text{-}YY}(\theta)=\frac{\sigma_0}{4\pi\sigma(\theta)}\sum_{L=2}^{4} a_L^{XX\text{-}YY}P_L^2(\cos\theta). \qquad (28)$$

The expansion coefficients a_L^K ($K=\sigma_0, XZ, ZZ, XX\text{-}YY$, and Y) in Eqs. (27) and (28) can be expressed in the following form:

$$a_L^K=\frac{1}{9\sigma_0}\sum_J\sum_{L_1,L_2}\sum_{l_1,l_2}\sum_{S_{\alpha_1},S_{\alpha_2}}\sum_{I_1,I_2} R_\xi(L_1,l_1,S_{\alpha_1},I_1;L_2,l_2,S_{\alpha_2},I_2)F_K(L_1,l_1,S_{\alpha_1},I_1;L_2,l_2,S_{\alpha_2},I_2;L,J), \qquad (29)$$

where $R_\xi=R_{\rm Re}$ for $K=XZ,ZZ,XX\text{-}YY$, and σ_0, and $R_\xi=R_{\rm Im}$ when $K=Y$. The $R_{\rm Re}$ and $R_{\rm Im}$ are the real and imaginary parts of the product of the radial integrals $\mathcal{R}_{L_1,l_1,S_{\alpha_1}}(I_1)\mathcal{R}^*_{L_2,l_2,S_{\alpha_2}}(I_2)$.

To find F_K in Eq. (29), we first write the product of transition amplitudes with total angular momentum J as the product of the radial transition amplitudes (for both of S- and D-state components of the deuteron and triton)

$$\sum_n M^J_{mm'_1,nn}(L_1,l_1,S_{\alpha_1},I_1)M^{*J}_{mm'_2,nn}(L_2,l_2,S_{\alpha_2},I_2)=\frac{1}{4\pi}\mathcal{R}_{L_1,l_1,S_{\alpha_1}}(I_1)\mathcal{R}^*_{L_2,l_2,S_{\alpha_2}}(I_2)\sum_L \sqrt{\frac{(L-|m'_2-m'_1|)!}{(L+|m'_2-m'_1|)!}}$$
$$\times G(L_1,l_1,S_{\alpha_1},I_1;L_2,l_2,S_{\alpha_2},I_2;J,L,m,m'_1,m'_2)P_L^{|m'_2-m'_1|}(\cos\theta). \qquad (30)$$

This defines G as a function of L, l, S_α, and I of the two transition amplitudes, as well as J. Note that the interference effect among the s, p, and d waves in analyzing powers within the same total angular momentum channel J is reflected in Eq. (30). The F_K coefficients in Eq. (29) are then defined as follows.

(i) F_{σ_0}: for the angular distribution of unpolarized cross section ($m'_1=m'_2=m'$),

$$F_{\sigma_0}(L_1,l_1,S_{\alpha_1},I_1;L_2,l_2,S_{\alpha_2},I_2;J,L)$$
$$=G(L_1,l_1,S_{\alpha_1},I_1;L_2,l_2,S_{\alpha_2},I_2;J,L,m,m',m'). \qquad (31)$$

(ii) F_{ZZ}: for the analyzing power A_{ZZ} ($m'_1=m'_2=m'$); one can use $m=1$ without losing generality which is the same for the other analyzing powers,

$$F_{ZZ}(L_1,l_1,S_{\alpha_1},I_1;L_2,l_2,S_{\alpha_2},I_2;J,L)$$
$$=G(L_1,l_1,S_{\alpha_1},I_1;L_2,l_2,S_{\alpha_2},I_2;J,L,1,1,1)$$
$$-2G(L_1,l_1,S_{\alpha_1},I_1;L_2,l_2,S_{\alpha_2},I_2;J,L,1,0,0)$$
$$+G(L_1,l_1,S_{\alpha_1},I_1;L_2,l_2,S_{\alpha_2},I_2;J,L,1,-1,-1). \qquad (32)$$

(iii) $F_{XX\text{-}YY}$: for the analyzing power $A_{XX\text{-}YY}$ ($m'_1=1$ and $m'_2=-1$),

TABLE III. Fitted values of the Legendre coefficients in comparison with those obtained from the experimental groups. The total unpolarized cross section σ_0 (mb) is an input.

E (keV)	30 Present	30 Expt	50 Present	50 Expt	70 Present	70 Expt	90 Present	90 Expt
a_0^{ZZ}	−0.0861	−0.0843	−0.1229	−0.1233	−0.1462	−0.1420	−0.1621	−0.1605
a_1^{ZZ}	0.0204	0.0205	−0.0576	−0.0556	−0.1441	−0.1433	−0.1807	−0.1711
a_2^{ZZ}	−0.8747	−0.8791	−0.8835	−0.8621	−0.8003	−0.7986	−0.8148	−0.8157
a_3^{ZZ}	0.1918	0.1966	0.1549	0.1335	0.0447	0.0431	0.0326	0.0320
a_4^{ZZ}	−0.0334	−0.0330	−0.0335	−0.0414	0.0420	−0.0382	−0.0693	−0.0631
a_1^{XZ}	0.0128	0.0137	−0.0521	−0.0483	−0.0726	−0.0823	−0.1245	−0.1212
a_2^{XZ}	−0.3923	−0.3965	−0.3882	−0.3861	−0.3801	−0.3793	−0.3613	−0.3620
a_3^{XZ}	0.0696	0.0532	0.0447	0.0410	0.0303	0.0310	0.0123	0.0159
a_4^{XZ}	−0.0010	−0.0012	−0.0038	−0.0071	−0.0099	−0.0106	−0.0108	−0.0107
a_2^{XX-YY}	−0.3585	−0.3526	−0.2941	−0.3041	−0.2671	−0.2678	−0.2466	−0.2411
a_3^{XX-YY}	0.0236	0.0284	0.0159	0.0201	0.0197	0.0173	0.0121	0.0125
a_4^{XX-YY}	0.0073	0.0069	0.0021	0.0014	0.0024	0.0000	0.0048	0.0000
a_1^{Y}	0.1677	0.1672	0.1764	0.1739	0.1769	0.1723	0.1770	0.1767
a_2^{Y}	−0.0252	−0.0247	−0.0246	−0.0260	−0.0343	−0.0341	−0.0374	−0.0352
a_3^{Y}	−0.0009	0.0000	−0.0094	0.0000	−0.0035	0.0000	0.0030	0.0000
a_4^{Y}	−0.0016	0.0000	−0.0016	0.0000	−0.0024	0.0000	0.0021	0.0000
σ_0(mb)	1.190	1.190	4.479	4.479	8.758	8.758	13.22	13.22
a_2	0.1295	0.1295	0.2191	0.2186	0.2728	0.2748	0.3169	0.3171
a_4	−0.0001	0.0000	0.0308	0.0307	0.0128	0.0127	0.0309	0.0308

$$F_{XX\text{-}YY}(L_1,l_1,S_{\alpha_1},I_1;L_2,l_2,S_{\alpha_2},I_2;J,L) = \frac{6}{\sqrt{(L-1)L(L+1)(L+2)}} \times G(L_1,l_1,S_{\alpha_1},I_1;L_2,l_2,S_{\alpha_2},I_2;J,L,1,1,-1). \quad (33)$$

(iv) F_Y: for the analyzing power A_Y ($m_1'=0$ and $m_2'=\pm 1$),

$$F_Y(L_1,l_1,S_{\alpha_1},I_1;L_2,l_2,S_{\alpha_2},I_2;J,L) = -\frac{\sqrt{2}}{\sqrt{L(L+1)}} \times \{G(L_1,l_1,S_{\alpha_1},I_1;L_2,l_2,S_{\alpha_2},I_2;J,L,1,0,1) - G(L_1,l_1,S_{\alpha_1},I_1;L_2,l_2,S_{\alpha_2},I_2;J,L,1,0,-1)\}. \quad (34)$$

(v) F_{XZ}: for the analyzing power A_{XZ},

$$F_{XZ}(L_1,l_1,S_{\alpha_1},I_1;L_2,l_2,S_{\alpha_2},I_2;J,L) = -\frac{3}{2}F_Y(L_1,l_1,S_{\alpha_1},I_1;L_2,l_2,S_{\alpha_2},I_2;J,L). \quad (35)$$

Notice that the angular momentum constraint $(-1)^{l_1+l_2}=(-1)^L$ is enforced via a C-G coefficient $C(l_1,l_2,L;0,0,0)$ implicit in G. Thus $a_1^{\sigma_0}=a_3^{\sigma_0}=0$ is ensured.

The 20 complex radial transition amplitudes listed in Table I are parametrized and labeled in the form $R(i)\exp(i\theta_i)\{i=1,20\}$. The 19 coefficients a_L^K in Eqs. (27) and (28) are labeled as $b(k)\{k=1,19\}$. Specifically, $b(k=1,2,3)=a_{0,2,4}^{\sigma_0}$; $b(k=4,\ldots,8)=a_L^{ZZ}$ $(L=0,\ldots,4)$; $b(k=9,\ldots,12)=a_L^{XZ}$ $(L=1,\ldots,4)$; $b(k=13,14,15)=a_L^{XX\text{-}YY}$ $(L=2,3,4)$; and $b(k=16,\ldots,19)=a_L^{Y}$ $(L=1,\ldots,4)$. Thus Eq. (29) can be reexpressed by

$$b(k)=\sum_{i,j=1}^{20} F(k,i,j)R(i)R(j)\cos(\theta_i-\theta_j) \quad \text{for } k=1,\ldots,15,$$

$$b(k)=\sum_{i,j=1}^{20} F(k,i,j)R(i)R(j)\sin(\theta_i-\theta_j) \quad \text{for } k=16,\ldots,19, \quad (36)$$

where $F(k,i,j)$ is the F function in Eq. (29). In Eq. (36), $R(i)R(j)$ is redefined to absorb the factor $1/9\sigma_0$ in Eq. (29) so as to make $R(i)$ dimensionless. Note that only the relative angles appear in Eq. (36). We take all the phases to be relative to that of $\mathcal{R}_{2,2,2}^{SS}(2)$. To fit to the experimental data, the χ^2 is given by

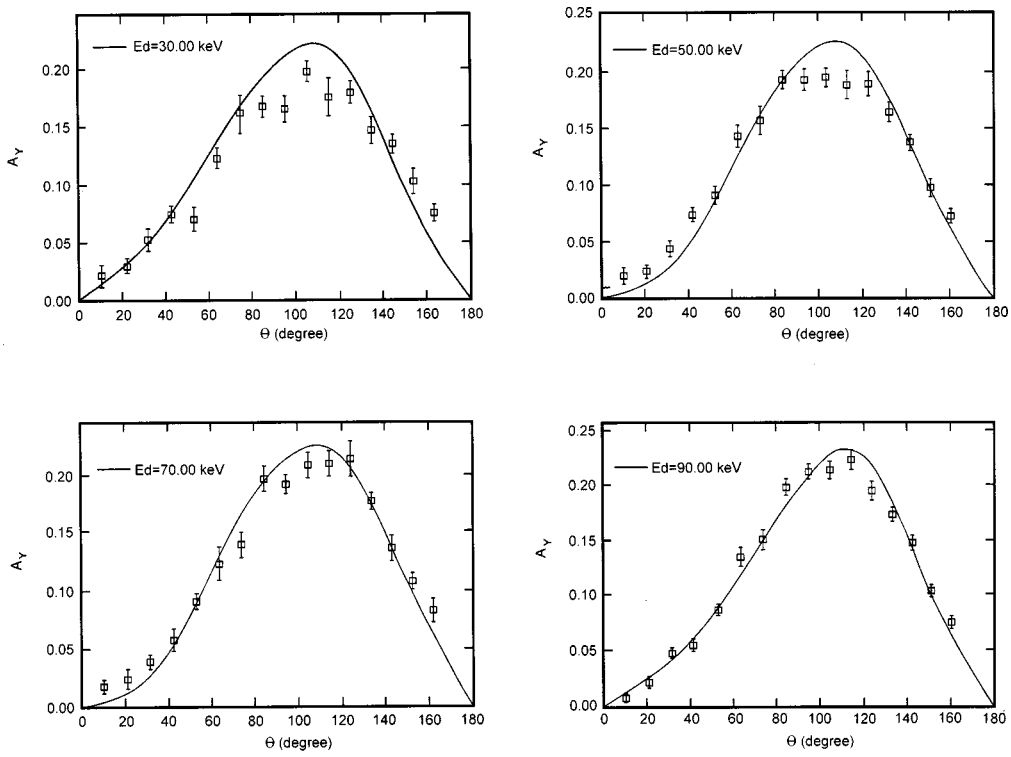

FIG. 3. Experimental angular distributions of the vector analyzing power A_Y for the $d(\vec{d},p)t$ reaction at $E_d=30$, 50, 70, and 90 keV are plotted as a function of the angles in degrees. The solid curves are the results of our fitting.

$$\chi^2=\frac{1}{N}\left(\left|\frac{a_2^{\sigma_0}(\text{expt})-a_2^{\sigma_0}}{\Delta a_2^{\sigma_0}}\right|^2+\left|\frac{a_4^{\sigma_0}(\text{expt})-a_4^{\sigma_0}}{\Delta a_4^{\sigma_0}}\right|^2+\sum_K\sum_{i=1}^{N_k}\left|\frac{A_K(\theta_i)_{\text{expt}}-A_K(\theta_i)}{\Delta A_K(\theta_i)}\right|^2\right), \tag{37}$$

where $a_{2,4}^{\sigma_0}(\text{expt})$ and $\Delta a_{2,4}^{\sigma_0}$ are the Legendre coefficients and the corresponding errors which are experimentally fitted to the unpolarized cross section $\sigma_0(\theta)$ [15]. For the vector and tensor analyzing powers we fit the experimental angular distributions [16] directly. In Eq. (37), the subscript K in A_K refers to XZ, ZZ, XX-YY, and Y. The number of data points is $N_{XZ}=17$, $N_{ZZ}=18$, $N_{XX\text{-}YY}=17$, and $N_Y=16$. Including $a_2^{\sigma_0}(\text{expt})$ and $a_4^{\sigma_0}(\text{expt})$, there are all together 70 data points at each energy. As far as the fitting parameters are concerned, all the theoretical quantities in Eq. (37) are expressed in terms of $b(k)$ in Eq. (36) where there are 20 radial transition amplitudes and 19 relative phase angles. Since in the process of fitting we fixed $a_0^{\sigma_0}=1$ by expressing $\mathcal{R}_{0,0,0}^{SS}(0)$ in terms of the other variables, this is a constraint. Therefore, we have totally 38 parameters. This leaves the degrees of freedom N in Eq. (37) to be 32.

The experimental data of the vector and tensor analyzing powers of the reaction $d(d,p)t$ in the manner of Tagishi *et al.* [12] are fitted at $E_{\text{lab}}=30$, 50, 70, and 90 keV separately. The Legendre coefficients $a_{2,4}^{\sigma_0}(\text{expt})$ for the unpolarized differential cross section of the same reaction and energies are taken from Brown and Jarmei [15]. The fitted results of the Legendre coefficients of the analyzing powers and $\sigma_0(\theta)$ are given in Table III together with those from the experimentally analyzed a coefficients. We see that they are very close to each other, agreeing to two significant figures in most cases. The experimental data for the analyzing powers (A_Y, A_{XZ}, A_{ZZ}, and $A_{XX\text{-}YY}$) and the unpolarized $\sigma_0(\theta)$ as evaluated from the experimentally fitted Legendre a coefficients are plotted in Figs. 3–7. Also plotted are our fits represented by the curves. We see from these figures that the experimental results are very well reproduced. The χ^2 per degree of freedom as defined in Eq. (37) is 1.15, 2.36, 3.13, and 2.28 at $E_d=30$, 50, 70, and 90 keV, respectively.

We should stress that the fitting is nonlinear. As can be seen from Eq. (36), $b(k)$ depends quadratically on the parameters $R(i)$ and the cosine of the angle differences $\theta_i-\theta_j$.

The fitted results of the dimensionless radial transition amplitudes for the reaction $d(d,p)t$ at $E_{\text{lab}}=30$, 50, 70, and 90 keV are listed in Table IV. The phase angles in degrees are shown in parentheses.

As we can see from Table IV, the largest radial transition amplitude is $\mathcal{R}_{2,0,2}^{SS}(2)$. This is the transition with $L_{\text{in}}=2$, $L_{\text{out}}=0$, and $S_{\text{in}}=2$ and is induced by the tensor force. However, as we shall see later, this does not contribute to the doubly polarized cross section $\sigma_{1,1}$.

IV. PREDICTION OF POLARIZED CROSS SECTIONS $\sigma_{1,1}$

We shall derive formulas that enable us to calculate the doubly polarized cross section $\sigma_{1,1}$ from the radial transition

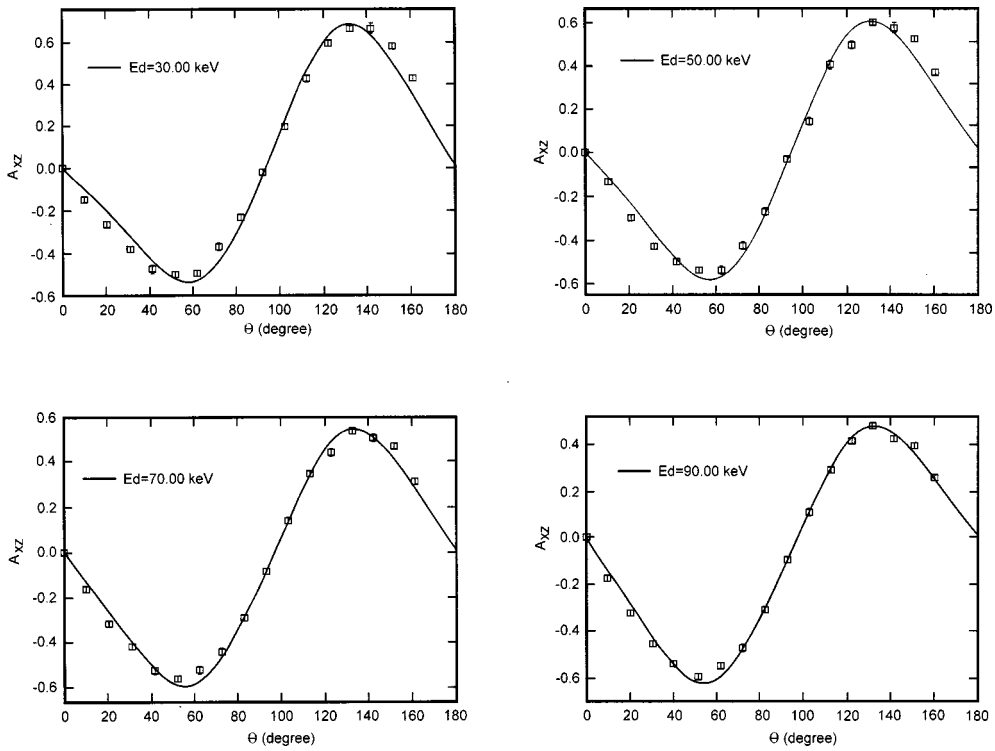

FIG. 4. The same as Fig. 3 for the tensor analyzing power A_{XZ}.

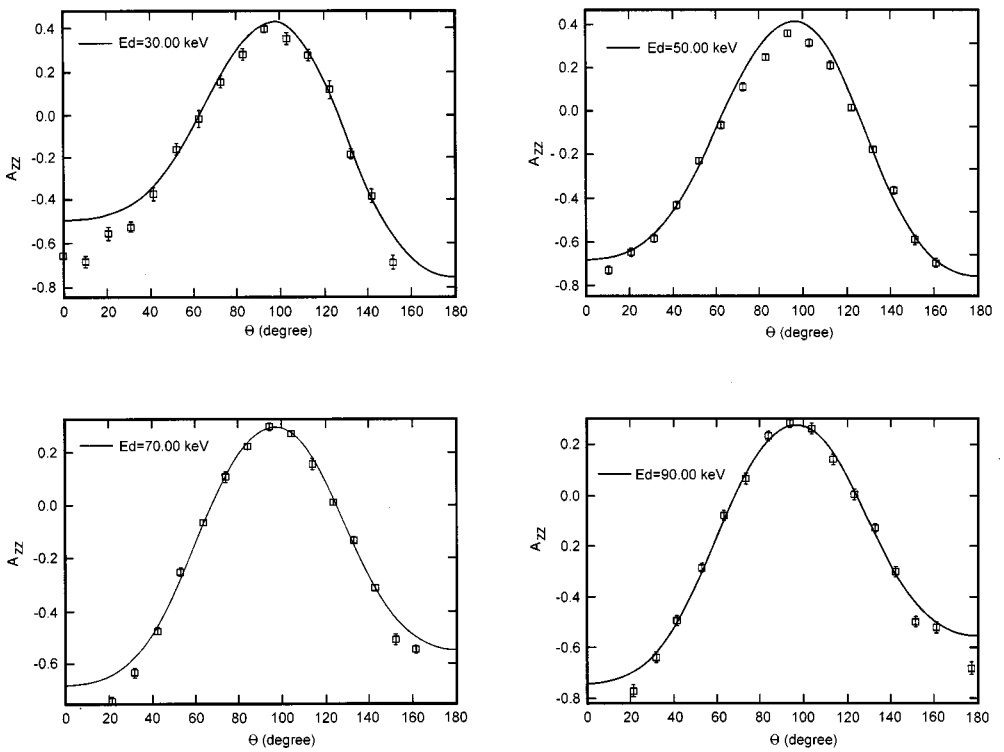

FIG. 5. The same as Fig. 3 for the tensor analyzing power A_{ZZ}.

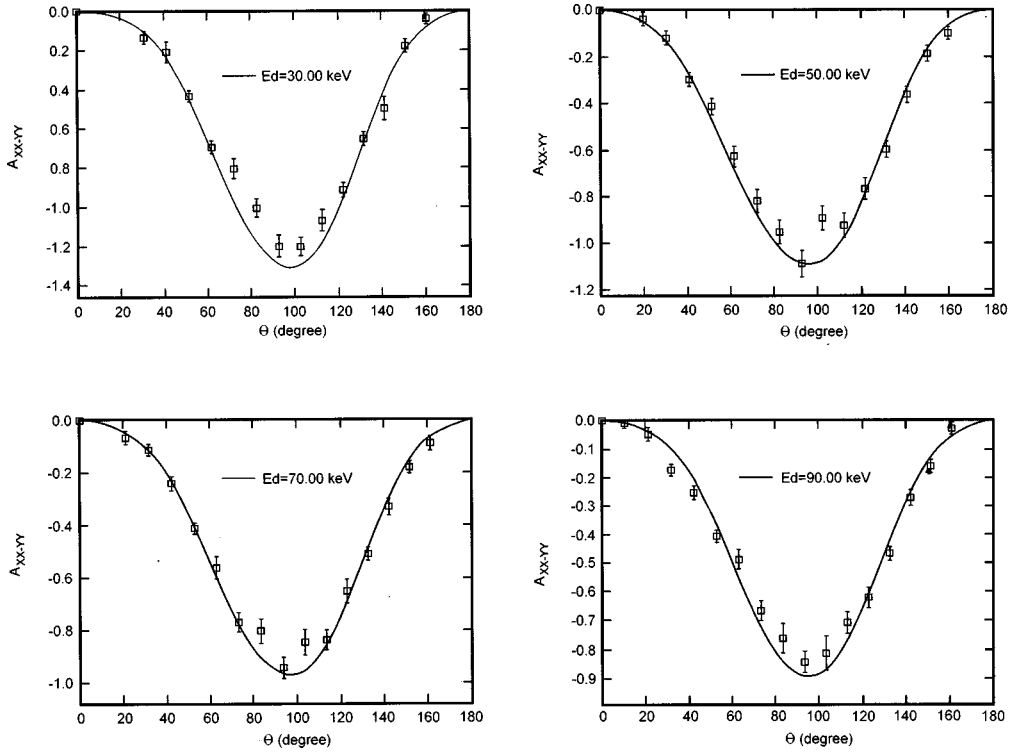

FIG. 6. The same as Fig. 3 for the tensor analyzing power $A_{XX\text{-}YY}$.

amplitudes obtained in Sec. III. From this, we can determine the ratio of $\sigma_{1,1}/\sigma_0$ as a function of the deuteron energy for the $d(d,p)t$ reaction.

A. Cross section of a polarized beam on a polarized target

The transition rate $\omega(i\rightarrow f)$ for a polarized beam on a polarized target can be described in the density-matrix form

$$\omega(i\rightarrow f)=\frac{1}{9}\mathrm{Tr}\left(M\left[\hat{I}+\frac{3}{2}\sum_i p_i S_i+\frac{1}{3}\sum_{kl} p_{kl}S_{kl}\right]\times\left[\hat{I}+\frac{3}{2}\sum_j p_j^T S_j^T+\frac{1}{3}\sum_{mn} p_{mn}^T S_{mn}^T\right]M^\dagger\right). \tag{38}$$

The definitions of all the symbols are given in Sec. III and the superscript T refers to the target. There are 81 terms in this equation, but the parity conservation forces 29 terms to be zero, which leaves 52 terms with detailed angular information. Since we are interested in the polarized *d-d* reaction in the fusion reactor environment, where the polarized deuteron velocity distribution is isotropic, we integrate the transition rate over the angles of $\beta=(0,\pi)$ and $\phi=(0,2\pi)$ to make the angular average. This further reduces the number of terms in Eq. (38). The transition rate for the perfectly polarized case ($p_z=p_{zz}=1$) at a given reaction energy can then be expressed as

$$\omega(i\rightarrow f)=\frac{1}{9}Tr(MM^\dagger)\left[1+\frac{3}{4}(C_{X,X}+C_{Y,Y}+C_{Z,Z})+\frac{1}{20}C_{ZZ,ZZ}+\frac{1}{60}C_{XX-YY,XX-YY}+\frac{1}{15}(C_{XY,XY}+C_{XZ,XZ}+C_{YZ,YZ})\right], \tag{39}$$

where the coefficients C's are the spin correlation coefficients. They are defined as follows:

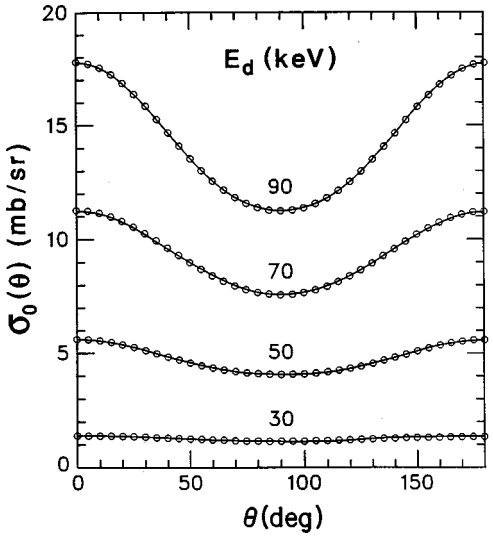

FIG. 7. Angular distribution of $\sigma_0(\theta)$ of the $d(d,p)t$ reaction at $E_d=30$, 50, 70, and 90 keV. The solid lines are from our fitting and the circles are the Legendre function fits of the experimental data.

TABLE IV. Fitted values of the dimensionless radial transition amplitudes with their phases in degrees shown in parentheses. All the phases are defined to be relative to that of $\mathcal{R}^{SS}_{2,2,2}(2)$.

$E_{\rm lab}$ (keV)	30	50	70	90
$\mathcal{R}^{SS}_{0,0,0}(0)$	1.130(−86.40)	0.878(−83.07)	0.874(−75.76)	0.722(−87.72)
$\mathcal{R}^{SS}_{2,0,2}(2)$	6.878(64.11)	7.193(721.91)	7.470(72.71)	7.193(72.26)
$\mathcal{R}^{SS}_{1,1,1}(0)$	0.386(−57.40)	0.361(−93.31)	0.137(−169.7)	0.204(−134.53)
$\mathcal{R}^{SS}_{1,1,1}(1)$	3.554(−24.50)	2.945(−11.01)	2.195(−6.530)	2.865(−19.09)
$\mathcal{R}^{SS}_{1,1,1}(2)$	2.387(0.000)	2.971(−135.64)	2.827(−117.54)	3.009(−138.99)
$\mathcal{R}^{SS}_{2,2,2}(1)$	1.291(140.9)	1.081(34.79)	0.701(73.21)	2.012(84.64)
$\mathcal{R}^{SS}_{2,2,2}(2)$	3.343(0.000)	3.610(0.000)	3.773(0.000)	3.572(0.000)
$\mathcal{R}^{SS}_{0,2,2}(2)$	1.026(−4.68)	1.066(114.58)	1.080(116.78)	1.078(−33.44)
$\mathcal{R}^{SS}_{2,2,0}(0)$	0.686(−63.08)	0.820(−38.23)	0.774(−5.39)	0.884(−12.25)
$\mathcal{R}^{SS}_{2,2,0}(1)$	2.502(−24.01)	1.887(12.34)	2.543(35.28)	1.380(25.17)
$\mathcal{R}^{SS}_{2,2,0}(2)$	0.624(−4.82)	0.137(8.27)	0.010(8.24)	0.647(4.03)
$\mathcal{R}^{SD}_{0,2,2}(0)$	0.603(−6.63)	1.056(10.23)	0.882(14.79)	0.815(17.48)
$\mathcal{R}^{SD}_{0,2,2}(1)$	0.321(−3.45)	0.003(−0.290)	0.290(−12.24)	0.457(−13.49)
$\mathcal{R}^{SD}_{0,2,2}(2)$	0.004(−0.17)	0.012(0.360)	0.021(0.000)	0.032(−10.29)
$\mathcal{R}^{DS}_{0,2,0}(0)$	0.513(27.84)	0.106(5.81)	0.115(11.45)	0.202(18.33)
$\mathcal{R}^{DS}_{0,2,0}(1)$	0.491(29.30)	0.094(5.78)	0.078(11.98)	0.172(18.21)
$\mathcal{R}^{DS}_{0,2,0}(2)$	0.490(27.86)	0.100(6.07)	0.101(11.56)	0.220(18.18)
$\mathcal{R}^{DS}_{0,0,2}(2)$	0.487(2.80)	0.101(5.72)	0.100(11.04)	0.218(18.37)
$\mathcal{R}^{DS}_{0,2,2}(1)$	0.511(29.54)	0.103(5.74)	0.090(11.57)	0.020(18.09)
$\mathcal{R}^{DS}_{0,2,2}(2)$	0.494(28.32)	0.030(5.79)	0.100(11.45)	0.220(18.39)

$$C_{\alpha,\beta}(\theta)=\frac{\mathrm{Tr}(MS_\alpha S_\beta^T M^\dagger)}{\mathrm{Tr}(MM^\dagger)},\qquad C_{ij,kl}(\theta)=\frac{\mathrm{Tr}(MS_{ij}S_{kl}^T M^\dagger)}{\mathrm{Tr}(MM^\dagger)},\tag{40}$$

$$C_{\alpha,ij}(\theta)=\frac{\mathrm{Tr}(MS_\alpha S_{ij}^T M^\dagger)}{\mathrm{Tr}(MM^\dagger)},$$

$$C_{ij,\alpha}(\theta)=\frac{\mathrm{Tr}(MS_{ij}S_\alpha^T M^\dagger)}{\mathrm{Tr}(MM^\dagger)},$$

where all of the operators are defined in Sec. III. The subscripts α, β, i, j, k, and l refer to X, Y, Z and the superscript T denotes the target particle. Substituting Eq. (40) into Eq. (39), the reaction cross section with a polarized beam and target is obtained as

$$\sigma_{1,1}=\int \omega(i\to f)d\Omega=\frac{1}{9}\int d\Omega\sum_{m,n}\left\{\frac{9}{5}|M_{m1,n1}|^2+\frac{9}{5}|M_{m-1,n-1}|^2+\frac{6}{5}\left|M_{m0,n0}\right|^2+\frac{3}{10}[|M_{m1,n-1}|^2+|M_{m-1,n1}|^2]\right.$$
$$\left.+\frac{9}{10}[|M_{m1,n0}|^2+|M_{m0,n1}|^2+|M_{m0,n-1}|^2+|M_{m-1,n0}|^2]\right\}.\tag{41}$$

It is interesting to observe that there is no P-wave contribution to the polarized deuteron fusion ($m=n=1$ and $S_{\rm in}=2$, $J=0,1,2$) due to the Pauli principle of two identical bosons in the entrance channel. The polarized deuteron fusion cross section can be written in terms of the radial transition amplitudes:

$$\sigma_{1,1}=\sum_J \sum_{L_{\mathrm{in}_1},L_{\mathrm{out}_1}} \sum_{L_{\mathrm{in}_2},L_{\mathrm{out}_2}} \sum_{S_{\mathrm{in}_1},S_{\mathrm{out}_1}} \sum_{I_1 I_2} \sum_{\lambda} R^{\lambda}_{\mathrm{Re}}(L_{\mathrm{in}_1},L_{\mathrm{out}_2},S_{\mathrm{in}_1},I_1;L_{\mathrm{in}_2},L_{\mathrm{out}_2},S_{\mathrm{in}_2},I_2)$$

$$\times\left[\frac{9}{5}Q^{\lambda}(L_{\mathrm{in}_1},L_{\mathrm{out}_1},S_{\mathrm{in}_1},I_1;L_{\mathrm{in}_2},L_{\mathrm{out}_2},S_{\mathrm{in}_2},I_2;J,1)+\frac{3}{10}Q^{\lambda}(L_{\mathrm{in}_1},L_{\mathrm{out}_1},S_{\mathrm{in}_1},I_1;L_{\mathrm{in}_2},L_{\mathrm{out}_2},S_{\mathrm{in}_2},I_2;J,-1)\right.$$

$$\left.+\frac{9}{10}Q^{\lambda}(L_{\mathrm{in}_1},L_{\mathrm{out}_1},S_{\mathrm{in}_1},I_1;L_{\mathrm{in}_2},L_{\mathrm{out}_2},S_{\mathrm{in}_2},I_2;J,0)\right], \tag{42}$$

where the superscript λ refers to the superscripts of the two radial transition amplitudes (S or D) from the multiplication of M and M^*. It labels the contribution from the different intrinsic wave functions of the deuteron and triton. $R^{\lambda}_{\mathrm{Re}}$ is defined in Eq. (29). For each λ, the Q function is defined by

$$\int d\Omega M_{1m',11}(L_{\mathrm{in}_1},L_{\mathrm{out}_1},S_{\mathrm{in}_1},I_1)M^*_{1m',11}(L_{\mathrm{in}_2},L_{\mathrm{out}_2};S_{\mathrm{in}_2},I_2)$$

$$\equiv\sum_J Q(L_{\mathrm{in}_1},L_{\mathrm{out}_1},S_{\mathrm{in}_1},I_1;L_{\mathrm{in}_2},L_{\mathrm{out}_2},S_{\mathrm{in}_2},I_2;J,m')R_{\mathrm{Re}}(L_{\mathrm{in}_1},L_{\mathrm{out}_1},S_{\mathrm{in}_1},I_1;L_{\mathrm{in}_2},L_{\mathrm{out}_2},S_{\mathrm{in}_2},I_2). \tag{43}$$

We see from Eqs. (42) and (43) that the imaginary part of the radial transition amplitude, R_{Im}, which contributes to A_Y in $\sigma_{1,0}(\theta)$, does not contribute to $\sigma_{1,1}$. Furthermore, we should stress that $\sigma_{1,0}(\theta)$ and $\sigma_{1,1}$ depend on different combinations of the radial transition amplitudes with different NN interactions, i.e., their dependence on I which labels the central, spin-orbit, and tensor interactions. This is clearly demonstrated by the fact that the F function in Eq. (29) for $\sigma_{1,0}(\theta)$ is different from the Q functions in Eq. (42) as far as their dependence on the NN interaction is concerned. Therefore, it is absolutely essential in the partial-wave analysis to separate out the radial transition amplitudes according to the tensor rank of the NN interaction in order to predict $\sigma_{1,1}$. On the other hand, one can sum up I_1 and I_2 (the dependence on the tensor rank of the NN interaction) in Eq. (29) before fitting the experiments as has commonly been done before. But by so doing, one loses the ability to predict $\sigma_{1,1}$.

Plugging the fitted radial integrals from Table IV into Eqs. (42) and (43), the fusion cross section of the polarized $d(d,p)t$ reaction is obtained at $E_d=30$, 50, 70, and 90 keV. Since the unpolarized cross-section σ_0 is well reproduced (see Table III and Fig. 7), we only give the predicted suppression ratio $\sigma_{1,1}/\sigma_0$ for the $d(d,p)t$ reaction in Table V. The suppression ratio $\sigma_{1,1}/\sigma_0$ is also plotted in Fig. 8.

B. Discussion of results

We see from Table V and Fig. 8 that the polarized $d(d,p)t$ reaction is essentially unsuppressed as compared to the unpolarized cross section at very low energy (i.e., $E_d=30$ keV), but becomes suppressed fairly quickly as E_d increases. By the time E_d reaches 90 keV, the suppression ratio has become about 22%. Modulo the presence of the Coulomb potential in the final state interaction of the $d(d,p)t$ reaction, we believe similar results hold for the $d(d,n)^3$He reaction. In the following discussion, we assume that this is the case. Comparing with our earlier DWBA calculation [9] which predicted a small suppression ratio (~8%) in this energy range, it is clear that the DWBA is inadequate at this low energy and has indeed underestimated the importance of the multistep transfer processes [10] that are included in the

TABLE V. Suppression ratio $\sigma_{1,1}/\sigma_0$ of the $d(d,p)t$ reaction at $E_d=30$, 50, 70, and 90 keV.

E_{lab} (keV)	30	50	70	90
$\sigma_{1,1}/\sigma_0$	0.866	0.564	0.331	0.219

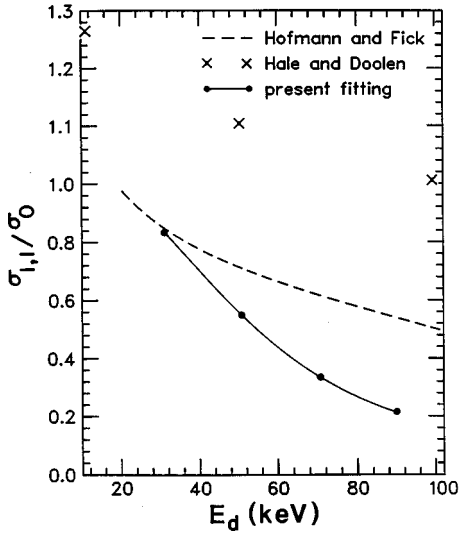

FIG. 8. The suppression ratio $\sigma_{1,1}/\sigma_0$ as a function of E_d. ● are our predictions. The dashed curve is the result of Hofmann and Fick [6] and × are the R-matrix predictions of Hale and Doolen [8].

TABLE VI. The breakdown of $\sigma_{1,1}/\sigma_0$ for the $d(d,p)t$ reaction according to the intrinsic states of the deuteron and triton at $E_d = 30$, 50, 70, and 90 keV. The σ_0 is taken as a whole; i.e., there is no breakdown in σ_0.

$E_{\rm lab}$ (keV)	30	50	70	90
total $\sigma_{1,1}/\sigma_0$	0.856	0.554	0.331	0.217
SS-SS	0.172	0.201	0.234	0.188
%	20.2	35.9	71.3	86.2
SD-SD	0.645	0.356	0.101	0.025
%	75.8	63.6	30.8	11.5
DS-DS	0.020	0.002	0.001	0.002
%	2.35	0.36	0.31	0.92
SS-SD+*SS-DS*	0.014	0.001	-0.008	0.003
%	1.65	0.17	-2.41	1.38

present partial-wave analysis. As compared to the resonating group calculation of $d(d,n)^3$He by Hofmann and Fick (also plotted in Fig. 8), we see that their result on the suppression ratio agrees with the present calculation at $E_d = 30$ keV, but becomes 3 times larger at $E_d = 90$ keV. As will be discussed later, despite the apparent difference at higher E_d, the RGM calculation has captured the dominant mechanism of the polarized reaction. But by either overestimating $\sigma_{1,1}$ or underestimating σ_0, it results in a mucher larger ratio at higher E_d. The *R*-matrix prediction for the $d(d,p)t$ reaction by Hale and Doolen [8] is also plotted in Fig. 8 for comparison. We see that their result shows no suppression at all in this energy range and is about 5 times larger than the present result at $E_d \sim 90$–100 keV. It is not clear where the discrepancy comes from, since both approaches fit the experimental data on $\sigma_0(\theta)$ and $\sigma_{1,0}$.

To examine the prediction of the suppression ratio further, we consider the breakdown of its contribution from different partial waves and different intrinsic states of the deuteron and triton. Listed in Table VI is the breakdown of $\sigma_{1,1}/\sigma_0$ according to the intrinsic wave functions of the deuteron and triton which are indicated as λ in Eq. (42). For example, *SD-SD* denotes the product of two transition amplitudes. One is with *S*-state component in the deuteron and *D*-state component in the triton, while the other is with *D*-state component in the deuteron and *S*-state component in the triton.

Some comments on the results in Table VI are in order.

(i) The *SS-SS* (both the deuteron and triton are in the *S*-state components) component contributes only 20% to the suppression ratio $\sigma_{1,1}/\sigma_0$ at $E_d = 30$ keV, but grows to 86% at $E_d = 90$ keV. The dominant contribution here is from the

TABLE VII. Contribution to $\sigma_{1,1}/\sigma_0$ from the tensor force term with $L_{\rm in}=0$, $L_{\rm out}=2$, $S_{\rm in1}=0$, $S_{\rm in2}=1$.

$E_{\rm lab}$ (keV)	30	50	70	90
SS-SS	0.152	0.126	0.094	0.074
%	17.7	22.7	28.3	35.8

TABLE VIII. Contribution to the ratio $\sigma_{1,1}/\sigma_0$ from the central force with $L_{\rm in}=0$, $L_{\rm out}=2$, $S_{\rm in1}=S_{\rm in2}=2$.

$E_{\rm lab}$ (keV)	30	50	70	90
SD-SD	0.910	0.695	0.356	0.093
%	106	124	107	41.7

s-wave incoming and *d*-wave outgoing channels with the tensor force. We show its contribution to the ratio in Table VII.

(ii) The contribution from the *SD-SD*–state component (both amplitudes are with *S*-state component in the deuteron and *D*-state component in the triton) dominates (76%) the suppression ratio at $E_d = 30$ keV, but quickly diminishes to only 10% at $E_d = 90$ keV. The dominant term here is from the *s*-wave incoming and *d*-wave outgoing channels with the central force and $S_{\rm in1}=S_{\rm in2}=2$. This agrees completely with the finding of the RGM calculation [6] at $E_d = 30$ keV. However, we find that the contribution from this transition amplitude dies down quickly as E_d increases, as illustrated in Table VI. This apparently is in contradiction with the RGM calculation [6] which finds this transition amplitude not to change much from $E_d = 40$ to 280 keV. Shown in Table VIII is the contribution from the major term, i.e., the *s*-wave incoming and *d*-wave outgoing channels with the central force and $S_{\rm in1}=S_{\rm in2}=2$. Note that the contributions from this term alone at $E_d = 30$, 50, and 70 keV are larger than the total $\sigma_{1,1}/\sigma_0$. It is the interference terms which reduce the contribution from this term and lead to the total *SD-SD* contribution to the suppression ratio in Table VI.

(iii) The smallness of the contribution from the *DS-DS*-state component shows that the *D* state in the deuteron is not nearly as important as the *D* state in the triton (and ^{3}He). This justifies our neglect of the exchange matrix element of the *D*-state deuteron as described in Sec. II.

(iv) The interference effect between the *S*- and *D*-state components are small as demonstrated by the small contribution from the *SS-SD*+*SS-DS* state component in Table VI.

V. SUPPRESSION OF THE SPIN-POLARIZED *d-d* REACTION RATE IN THERMAL FUSION

Since the present study is prompted by the interest of a possible neutron-lean fusion reactor based on polarized *D*-^{3}He fuel, we explore the question of neutron suppression in the thermal fusion reactor environment as a function of the deuteron energy.

The major source of neutrons in the *D*-^{3}He reactor consists of the primary reaction $d(d,n)^3$He and the secondary reaction $d(t,n)\alpha$ where the tritons are produced from the $d(d,p)t$ reaction. The reaction rate of the $d(d,p)t$ [or $d(d,n)^3$He] reaction of the plasma is defined as $R=\frac{1}{2}n_d^2 S$, where S stands for the reaction rate $\langle \sigma v \rangle$ for the *dd* fusion reaction, n_d refers to the deuteron density in the plasma, and the 1/2 factor takes care of the double countings due to identical particles in the reacting pairs. The reaction rate $\langle \sigma v \rangle$ of

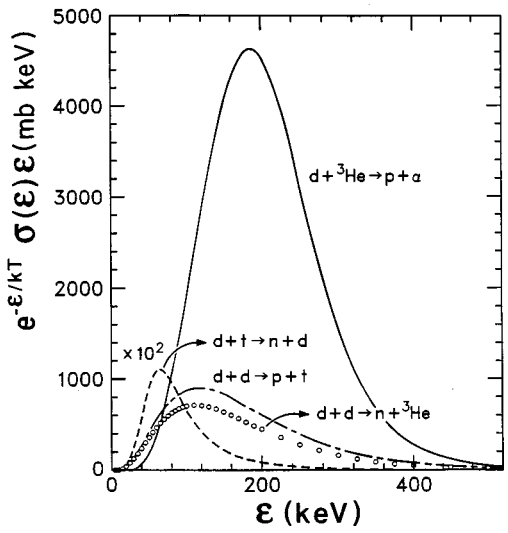

FIG. 9. The integrands of the reaction rate $\langle \sigma v \rangle$ in Eq. (44), i.e., $e^{-\varepsilon/KT}\varepsilon\sigma(\varepsilon)$ for the unpolarized reactions $d+{}^3\mathrm{He}\rightarrow p+\alpha$, $d+d\rightarrow p+t$, $d+d\rightarrow n+{}^3\mathrm{He}$, and the secondary reaction $d+t\rightarrow n+\alpha$ are plotted as a function of the center-of-mass energy of the reaction pairs.

the reacting particles with an isotropic and Maxwellian velocity distribution at temperature T can be expressed as

$$\langle \sigma v \rangle = \frac{2}{KT}\sqrt{\frac{2}{\pi KT\mu}}\int e^{-\varepsilon/KT}\varepsilon\sigma(\varepsilon)d\varepsilon, \qquad (44)$$

where μ and ε stand for the reduced mass and the center-of-mass energy of the reaction pairs, while σ is the effective reaction cross section.

In order to study the question of neutron suppression, we first plot the unpolarized fusion reaction rates $\langle \sigma v \rangle$ as a function of the center of mass energy of the reaction pairs. As shown in a conceptual design of a D-^{3}He fueled tandem mirror reactor [3,4], the optimal temperature is found to be $\sim$75 keV. Here we shall use T at 60 keV as an illustration. Hence, the reaction rates of the unpolarized reactions $d+{}^3\mathrm{He}\rightarrow p+\alpha$, $d+d\rightarrow p+t$, $d+d\rightarrow n+{}^3\mathrm{He}$, and the secondary reaction $d+t\rightarrow n+\alpha$ are plotted in Fig. 9 for $T=60$ keV. First we notice that the reaction rate $d+t\rightarrow n+\alpha$ is muchlarger than the others. However, since the triton in this secondary reaction comes from the reaction $d+d\rightarrow p+t$, it would be sufficient to suppress the $d(d,p)t$ and $d(d,n)^3$He reactions in order to reduce the neutron yield. As we turn our attention to the latter reactions, it is clearly seen in Fig. 9 that the dominant reaction rates for the neutron production lie roughly between 40 keV and 300 keV for the dd center-of-mass energy. Thus, in order to reliably predict the neutron suppression in a polarized D-^{3}He reactor operating at $T=60$ keV, one needs to know the suppression ratio $\sigma_{1,1}/\sigma_0$ in this energy range. Since our present study covers the range between 15 keV and 45 keV ($E_d=30$–90 keV) only, we are not in a position to make a prediction until there are more accurate experimental data available in this energy range. In this regard, we hope that the experimental data for the beam-polarized $d(d,p)t$ cross section will become available in the laboratory energy range $E_d=100$–600 keV. Of course it would be better still to have the both beam and target polarized reaction cross section. We can use it directly in the reactor study of neutron suppression and, furthermore, it would be useful to check the prediction of our partial-wave analysis.

VI. CONCLUSION

In summary, we have initiated a partial-wave analysis of the dd fusion reaction $d(d,p)t$ which separates out the radial transition amplitudes according to the tensor rank of the NN interaction, i.e., the central, spin-orbit, and tensor interactions. This way, it becomes feasible to extract the relevant radial transition amplitudes by fitting the angular distributions of the tensor and vector analyzing powers $A_{XZ}(\theta)$, $A_{ZZ}(\theta)$, $A_{XX\text{-}YY}(\theta)$, and $A_Y(\theta)$, and the unpolarized cross section $\sigma_0(\theta)$. We have done so for the $d(d,p)t$ reaction at $E_d=30$, 50, 70, and 90 keV. The partial wave is expanded to d waves in both the entrance and exit channels. The D-state components in the triton and the deuteron are also included. The doubly polarized fusion cross section $\sigma_{1,1}$ is predicted from these radial transition amplitudes. We should stress that this is possible only when the radial transition amplitudes are separated out according to the tensor rank of the NN interactions. We found that the suppression ratio $\sigma_{1,1}/\sigma_0$ is close to unity at $E_d=30$ keV and goes down to about 20% at $E_d=90$ keV. We verified that little or no suppression (large suppression ratio) of the polarized reaction at very low E_d is caused mainly by the central force in the s-wave incoming and d-wave outgoing channels with the outgoing triton in the intrinsic D-state component. However, the polarized cross section from this transition amplitude is quickly canceled out by the interference terms from other amplitudes as E_d increases.

We have studied the issue of neutron suppression in the fusion rector context with the polarized D-^{3}He fuel. In plotting out the reaction rate $\langle \sigma v \rangle$ for the unpolarized $d(d,p)t$ and $d(d,n)^3$He reactions at $T=60$ keV as a function of the deuteron energy, we realize that the important range for suppressing the dd fusion reaction is actually from $E_d=80$ keV to 600 keV. We hope that experimental data on the beam-polarized cross section $\sigma_{1,0}(\theta)$ in this energy range will become available in the future so that we can make a prediction of the suppression ratio $\sigma_{1,1}/\sigma_0$ in this energy range. This information is essential to answering the question about neutron suppression in a fusion reactor setting.

ACKNOWLEDGMENTS

This work was partially supported by DOE Grant Nos. DE-FG05-84ER40154 and DE-FC02-91ER5661. The authors would like to thank H. Paetz gen. Schieck, Edward J. Ludwig, and Y. Tagishi for providing us their experimental data. We are grateful to M. McEllistrem for reading over the manuscript. One of the authors (J.S.Z.) is indebted to Prof. Z. X. Sun for introducing the subject of polarization to him.

[1] R.M. Kulsrud, H.P. Furth, E.V. Valeo, and M. Goldhaber, Phys. Rev. Lett. **40**, 1248 (1982).
[2] S. Tamor, G.W. Shuy, and K.F. Liu, Bull. Am. Phys. Soc. **27**, 922 (1982).
[3] G.W. Shuy, A.E. Dabiri, and H. Guraol, Fusion Technol. **9**, 459 (1986).
[4] G.W. Shuy and D. Dobrott, ''Deuterium-Based Fuel Cycle Optimization,'' APPAT-20, Report, Science Applications International Corporation, 1983.
[5] B.P. Ad'yasevich and D.E. Fomenko, Sov. J. Nucl. Phys. **9**, 167 (1969); B.P. Ad'yasevich *et al.*, *ibid.* **33**, 313 (1981).
[6] H.M. Hofmann and D. Fick, Phys. Rev. Lett. **52**, 2038 (1984).
[7] G.M. Hale, in Proceedings of the Polarized Fusion Fuel Workshop, University of Wisconsin, 1983, University of Wisconsin Report No. UWFDM-503, 1983.
[8] G.M. Hale and G.D. Doolen, Los Alamos Report No. LA-9971-MS, 1984.
[9] J.S. Zhang, K.F. Liu, and G.W. Shuy, Phys. Rev. Lett. **57**, 1410 (1986); **55**, 1649 (1985).
[10] S. Abu-Kamer, M. Igarashi, R.C. Johnson, and J.A. Tostevin, J. Phys. G **14**, L1 (1988).
[11] H. Paetz gen. Schieck, B. Becker, R. Randermann, S. Lemaitre, P. Niessen, R. Reckenfelderbaumer, and L. Sydow, Phys. Lett. B **276**, 290 (1992).
[12] Y. Tagishi, N. Nakamoto, K. Katoh, J. Togawa, T. Hisamune, T. Yoshida, and Y. Aoki, Phys. Rev. C **46**, 1155 (1992).
[13] K.A. Fletcher Ph.D. thesis, University of North Carolina at Chapel Hill, 1992 (unpublished).
[14] G.G. Ohlson, Rep. Prog. Phys. **35**, 717 (1972).
[15] R.E. Brown and N. Jarmei, Phys. Rev. C **41**, 1391 (1990).
[16] Y. Tagishi (private communication).